Results in Engineering 15 (2022) 100553

Contents lists available at ScienceDirect

Results in Engineering

journal homepage: www.sciencedirect.com/journal/results-in-engineering

Synthesis and characterization of an activated carbon-supported silver-silica nanocomposite for adsorption of heavy metal ions from water

James Nyirenda *, George Kalaba, Onesmus Munyati

Department of Chemistry, School of Natural Sciences, The University of Zambia, P. O Box 32379, Lusaka, Zambia

ARTICLE INFO

Keywords:
Adsorption
Activated carbon
Nanocomposite
Isotherms
Kinetics
Thermodynamics

ABSTRACT

We report synthesis and characterization of an activated carbon-supported silver-silica nanocomposite (AC-Ag-SiO_2) for removal of Cu^{2+}, Pb^{2+}, Cd^{2+} and Zn^{2+} ions from single and multi-metal aqueous solutions. Characterization experiments included Atomic force microscopy (AFM), Ultraviolet–visible spectrophotometry (UV–Vis), Fourier transform Infrared spectrophotometry (FT-IR) and X-ray diffraction (XRD) analysis. Adsorption of heavy metals onto the composite strongly depended on contact time (280 min maximal), adsorbent dosage (0.1–0.4 g), solution pH (5.5 ± 0.5 maximal), temperature (298–328 K) and initial metal concentration. Equilibrium data were fitted to the Langmuir, Freundlich and Temkin isotherm models. Kinetic data were fitted to pseudo-first-order and pseudo-second-order kinetic models with the Freundlich isotherm model ($R^2 > 0.99$) and pseudo-second-order kinetic mode ($R^2 > 0.999$) providing a better fit to the experimental data. The maximum adsorption capacity was found to be 84.75 ± 0.24, 81.30 ± 0.2, 87.72 ± 0.96 and 81.97 ± 0.39 mg/g for Cu^{2+}, Pb^{2+}, Cd^{2+} and Zn^{2+} ions, respectively. The obtained values of thermodynamic parameters such as ΔG° (−13.72 ± 0.20 to −5.45 ± 0.35 kJ/mol), ΔH° (95.10 ± 14.33 to 162.4 ± 27.17 J/K.mol), and ΔS° (22.81 ± 4.50 to 39.12 ± 8.70 kJ/mol) showed that the adsorption process of Cu^{2+}, Pb^{2+}, Cd^{2+} and Zn^{2+} ions onto AC-Ag-SiO_2 composite was spontaneous, feasible, endothermic and physical in nature. Regeneration studies suggested that AC-Ag-SiO_2 composite could be reused effectively with no statistical significance among the cycles ($p > 0.9$ for all the four metal ions).

1. Introduction

Water is an especially important component of metabolic processes as well as an essential solvent. Thus, the need to have clean and fresh water for the existence of life cannot be overemphasized. Even so, the world's sources of fresh water are being threatened by microbiological, organic and inorganic pollutants such as pathogens [1], dyes [2], persistent organic pollutants (POPs) [3], pharmaceuticals [4] and heavy metals [5]. The release of heavy metals in fresh water sources is of significant concern globally because of their potential adverse effects on both human health and the environment [6]. In Zambia, some residents in mining areas of the Copperbelt have been reported to suffer from many health complication due to consumption of water contaminated with heavy metals [7]. Heavy metals are natural components of the earth's crust, they can't be degraded or destroyed and they have a tendency to accumulate for a long time [8,9] and as a result they are considered to be the most important pollutant in source and treated water [10]. Zinc, lead, cadmium and copper are among the heavy metal pollutants highly studied in Zambia [11–15]. Increased mining and agricultural activities have resulted in an increased availability of metallic substances in natural water sources [16–19]. The recommended amount of cadmium, zinc, copper and lead in portable water by World Health Organization is 2 ppm, 0.01 ppm, 0.003 ppm and 3 ppm, respectively [97]. The accumulation of these metals in the human body can cause nausea, neurotoxicity, hypertension, cancer, cell damage, kidney and liver dysfunction [20,21].

Therefore, the development and fabrication of modern technologies for removing heavy metals from water is fundamental. Many technologies for heavy metal removal such as ion exchange process [22], electrochemical deposition [9], membrane separation [23], ultra-filtration [21] and many others have been used. Although the effectiveness of these techniques have been proved sufficiently, they still present many draw backs such as high energy requirement, large volume of sludge production and complex operation [24–27].

The adsorption process is among the most promising technologies for the removal of pollutants from both fresh water and wastewater

* Corresponding author.
E-mail addresses: jamesn7414@gmail.com, nyirendaj@unza.zm (J. Nyirenda).

https://doi.org/10.1016/j.rineng.2022.100553
Received 16 May 2022; Received in revised form 14 July 2022; Accepted 17 July 2022
Available online 2 August 2022

respectively. The technique has been used by researchers for many years and the effectiveness of various adsorbents have been demonstrated in source water and wastewater application, some of them are; silica [28], activated carbon [29,30], nanomaterials [31,32], fly ash [33], aluminosilicate [34], composites [35]; [98]) and clay [36]. Activated carbon (AC) is commonly employed in many adsorption studies and is characterized by high surface area, physicochemical stability and porosity [17, 28]. Commercially available activated carbon offers shorter treatment time, requires lower level expertise but it is expensive due to the high cost of the activation process and the raw materials are obtained from coal, lignite as well as petroleum coke which are all non-renewable environmentally unsound substances [37]. Thus, in this study, nanomaterials (silver and silica nanoparticle) were incorporated onto activated carbon derived from renewable, abundant and low-cost materials originated from waste biomass, a valuable resource even for potential chemical feedstock [38]to produce a composite and to assess the composite's adsorptive properties.

2. Materials and methods

Chemicals: Cadmium nitrate tetra-hydrate (Cd $(NO_3)_2.4H_2O$), Zinc nitrate hexa-hydrate (Zn $(NO_3)_2.6H_2O$), Copper (Hamwiinga et al.) sulphate ($CuSO_4$), lead (Hamwiinga et al.) nitrate (Pb $(NO_3)_2$), sodium silicate (Na_2SiO_3), ammonium hydroxide (NH_4OH), hydrochloric acid (HCI), sodium hydroxide (Ikenaka et al.), ethanol (C_2H_5OH), silver nitrate ($AgNO_3$), native starch, sulphuric acid (H_2SO_4)98%, and distilled water. All the reagents were analytical grade.

Instrumentation: PerkinElmer AAnalyst 400 Atomic absorption spectrophotometer was used to measure the concentrations of heavy metals before and after adsorption. A Shimadzu 2000 UV-VIS spectrophotometer in scanning mode between 200 nm and 800 nm was used to acquire UV–Vis spectra with distilled water as a reference. FT-IR analysis was done using Shimadzu IRSpirit spectrophotometer, AFM experiments were performed using a Bruker Dimension Icon AFM in scanAsyst imaging mode and XRD analysis was conducted using ARL EQUINOX 1000 X-Ray Diffractometer.

2.1. Sample preparation

2.1.1. Preparation of maize cob activated carbon (AC-MC)

Dry maize cobs (Ho and McKay) were reduced to 2 mm particle size consistence. The raw material was pre-heated at 383 K for 2 h in a Carbolite AAF 11/7 Furnace at a heating rate of 283 K/min. Chemical activation with 50% sulphuric acid [39–41] was carried out using an impregnation method as described by Nyirenda et al. [42].

2.1.2. Preparation of silica nanoparticles (SiO_2 NPs)

A 3:1 Ammonium hydroxide-ethanol mixture was prepared to which dissolved sodium silicate was added drop by drop. After aging for 2 h the solution was centrifuged and the product was washed severally with distilled water and dried to obtain silica nanoparticles (SiO_2 NPs) [43].

2.1.3. Preparation of silver nanoparticles (Ag NPs)

In the present study, the preparation of powdered silver nanoparticles (Ag NPs) adopted the chemical reduction method by Ref. [44] with modification. Thus, 1.5 g of sodium hydroxide (Ikenaka et al.) was dissolved in 80 ml of distilled water and 4.72 g starch added to the solution at 343 K. An equal amount of silver nitrate ($AgNO_3$) was dissolved in 20 ml distilled water and added slowly to the alkaline solution under vigorous stirring. The reaction was kept for 60 min at pH 12. Finally, 100 ml of absolute ethanol was added slowly to the solution to precipitate silver nanoparticles. The precipitate was collected by centrifugation, then washed with ethanol and dried.

2.1.4. Preparation of the AC-Ag-SiO_2 nanocomposite

The scheme for the synthesis of AC-Ag-SiO_2 nanocomposite.

Fig. 1 shows the synthesizing of activated carbon-supported silver and silica composite (AC-Ag-SiO_2) composite. About 10 g of activated carbon and 4.75 g silica nanoparticles were mixed with 100 ml of colloidal solution of silver nanoparticles (50% based on weight of activated carbon). The solution was heated at 343 K with constant stirring until the formation of a gel. The gel was dried overnight at 353 K and calcined at 573 K for 2 h to yield a composite of activated carbon-silver-silica (AC-Ag-SiO_2).

2.2. Preparation of stock solution

Stock solutions of 1000 mg/L metal ion concentrations were prepared by dissolving a specific mass of metal salt. Aqueous solutions of the standards were further prepared by serial dilution with distilled water.

3. Results and discussion

3.1. Characterization

3.1.1. UV–visible and FTIR analysis

In this study, the silver nanoparticles (Ag NPs) were reduced and stabilized by alkali dissolved starch. Observation of the colour change from a clear colourless solution to a dark brown colour indicated the formation of the silver nanoparticles. The conduction band and valence band in silver nanoparticles lie very close to each other and the electrons move freely [45]. These results into a surface-plasmon resonance absorption band [46]. A wavelength scan in the UV–Vis spectra exhibited a characteristic absorption peak at 412 nm [47] (Fig. 2a) which corresponds to the Surface Plasmon Resonance (SPR) of silver nanoparticles. This observation indicates clearly the reduction of silver using alkali dissolved starch and is in agreement with the results obtained by Ref. [44].

In the case of silica nanoparticles, an absorption peak was obtained at 279 nm (Fig. 2a). The UV–Vis spectrum of silica nanoparticles (SiO_2 NPs) is in agreement with the results obtained by Refs. [48–50].

3.1.2. FT-IR analysis of SiO_2 NPs, Ag NPs, MC-AC and AC-Ag-SiO_2 composite

Silica nanoparticles were confirmed by FT-IR analysis (Fig. 2b). The bands at 803 and 444 cm^{-1} were assigned to Si–O–Si stretching and Si–O–Si bending vibrations, respectively as reported by Ref. [51]. The band at 957 cm^{-1} is associated with Si–OH groups; the band's existence is due to high concentrations of silanol groups [52]. Absorption bands at 1066 cm^{-1} are associated with asymmetric stretching vibrations of siloxane (Si–O–Si) [49]. The peaks at 3443 and 1636 cm^{-1} are attributed to O–H stretching bands of the surface silanol groups and the remaining absorbed water [51,53]. The analysis from FT-IR confirms that the silica nanoparticles were successfully synthesized.

The FT-IR spectra of silver nanoparticles showed an intense broad band at 3238 cm^{-1} which is attributed to carboxylic acid (Khamkure et al.) stretching vibration of starch [54]and asymmetric stretching of C–H band at 2930 cm^{-1} [55]. The absorption band at 1590 cm^{-1} was attributed to the water adsorbed in the amorphous region of starch, and the band at 1339 cm^{-1} was assigned to the angular deformation of C–H [56]. The absorption bands at 1014 cm^{-1} is because of O–H bending vibrations of starch [55].

FT-IR analysis of the activated maize cob confirms a band at around 3010 cm^{-1} [57] which can be assigned to O–H stretching vibration of carboxylic group. The band at 1784 cm^{-1} relates to C═O stretching of carboxylic group [39]. The band at 1556 cm^{-1} confirms the presence of C═C stretching vibration in aromatic rings [39,58], and the band around 1185 cm^{-1} can be assigned to C–O or C–O–C stretching vibrations [59]. The presence of O–H and C═O bands suggests that the maize cob was activated by sulphuric acid.

The surface functional group of AC-Ag-SiO_2 composite were also

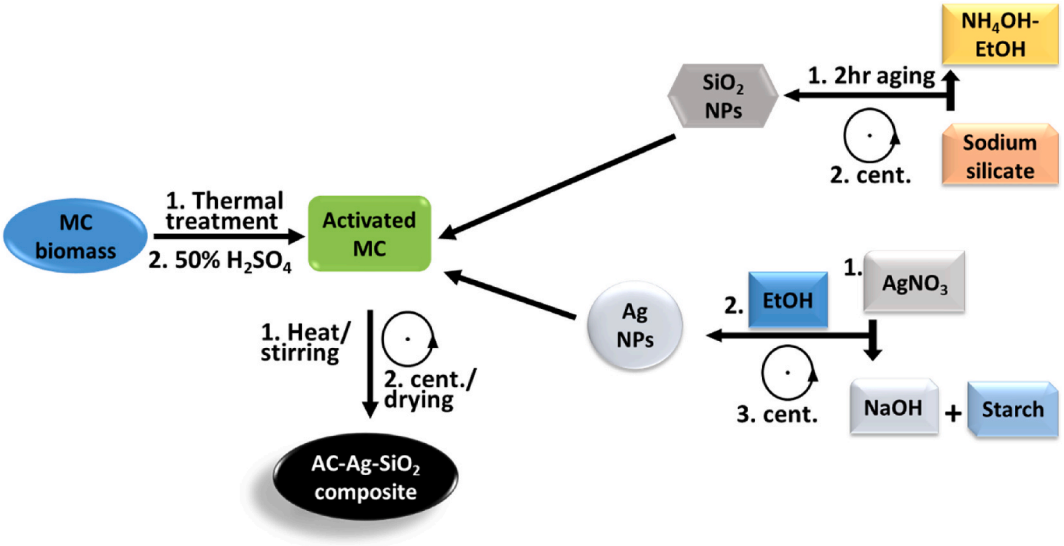

Fig. 1. Shows the schematic presentation of the synthetic pathway for the activated carbon-silver-silica composite.

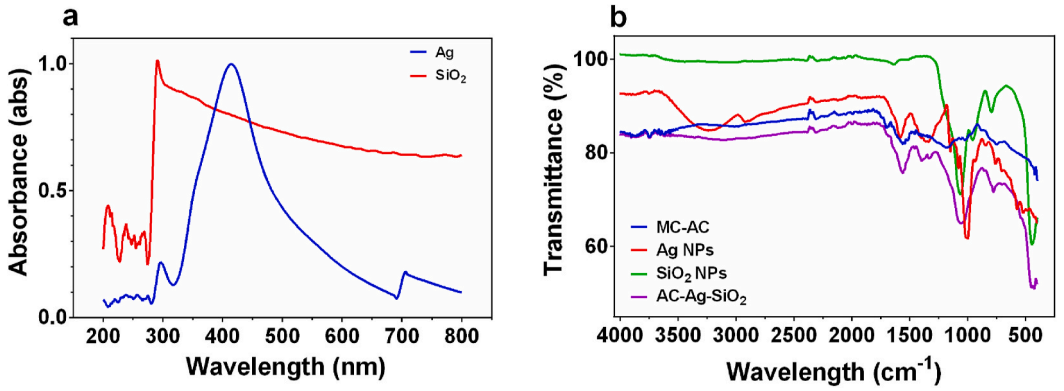

Fig. 2. UV–Vis and FT-IR spectra of SiO_2 NPs, Ag NPs, MC-AC and AC-Ag-SiO_2 composite.

identified by FT-IR spectral analysis, the peaks at 444, 803, 1066, 1396, 1556, 3010 cm^{-1} confirmed the presence of Si–O–Si stretching, Si–O–Si bending, asymmetric stretching vibrations of siloxane (Si–O–Si), C–H deformation, C═C stretching vibrations and O–H stretching vibrations, respectively.

3.1.3. AFM studies of silver and silica nanoparticles

The AFM analysis was conducted on silver and silica nanoparticles to study the surface morphology (shape and size) of silver and silica nanoparticles. The AFM analysis were conducted in contact mode [60,61] and are shown in Fig. 3a and b. The AFM analysis showed that silver nanoparticles were predominantly spherical shaped with particle size between 17 and 26 nm. Silica nanoparticles were spherical with particle size between 55 and 80 nm and were in agreement with [43,62,63].

3.1.4. XRD analysis

The crystalline nature of the synthesized silver nanoparticles was studied using X-ray diffraction as shown in Fig. 4a. The spectra shows peaks located at 44.99, 54.53, 77.50° which agrees well with the (200), (142), (311) planes for silver nanoparticles [64,65]. The XRD of silica nanoparticles (Ag NPs) is shown in Fig. 4b. The pattern of silica nanoparticles shows that they are mainly amorphous in nature with the broad

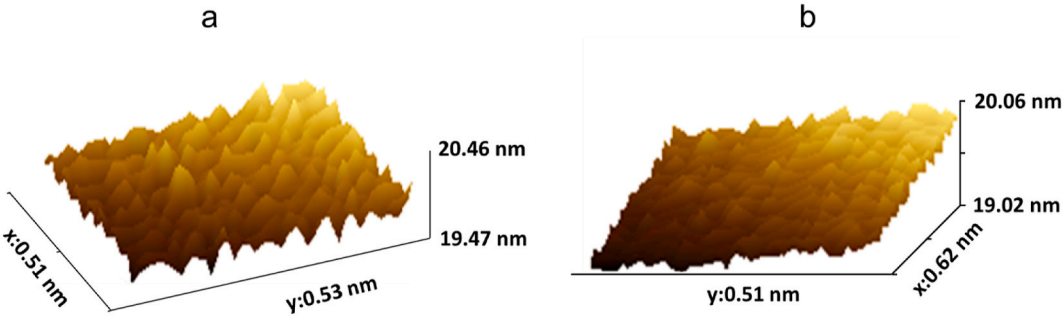

Fig. 3. AFM image of the synthesized (a) silver (Ag NPs), (b) silica (SiO_2 NPs) nanoparticles.

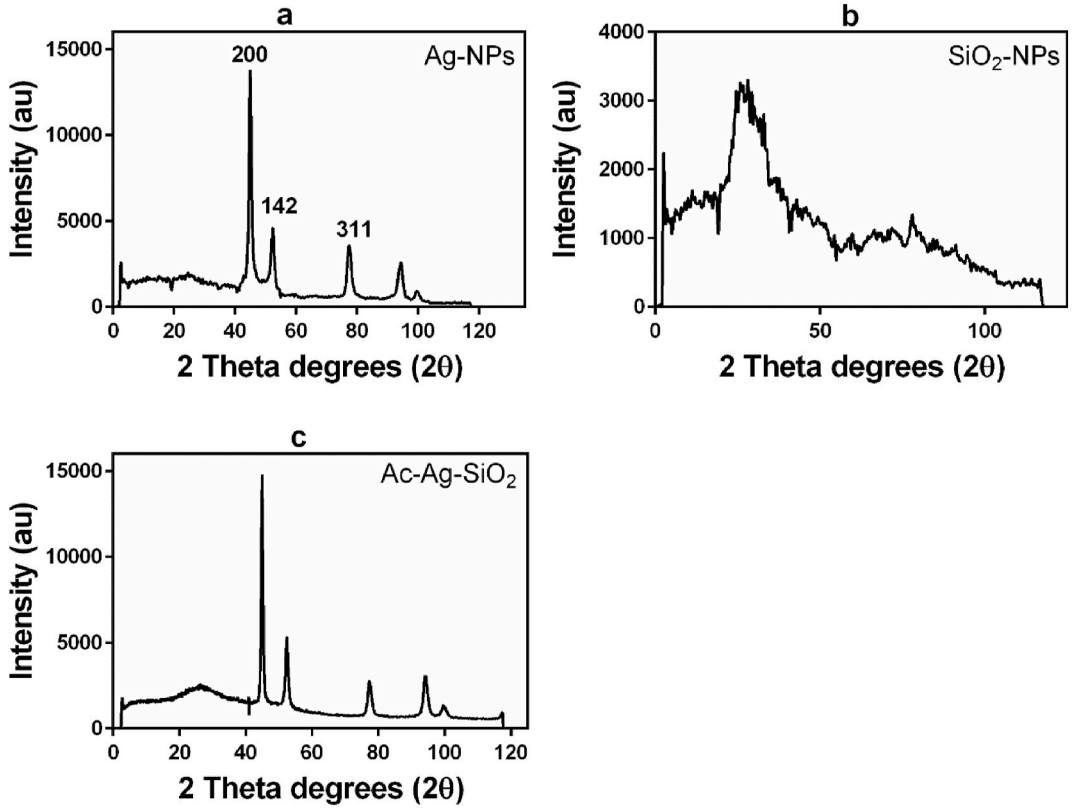

Fig. 4. XRD spectra of the synthesized (a) silver (Ag NPs), (b) silica (SiO_2) nanoparticles and (c) AC-Ag-SiO_2 composite.

peak in the range of 20° - 38°. The results are in agreement with [43,66,67]. From the spectra of AC-Ag-SiO_2 composite (Fig. 4c), it can be concluded that silver and silica nanoparticles were loaded in the composite.

3.2. Adsorption experiments

Adsorption efficiency (%) and adsorption capacity at equilibrium (q_e) ([103] [68], were determined using equation (1) and (2);

$$\text{Adsorption efficiency } (\%) = \frac{(C_o - C_e) \times 100}{C_o} \quad (1)$$

$$\text{Adsorption capacity } (q_e) = \frac{(C_o - C_e) \times V}{m} \quad (2)$$

where C_o (mg/L) is the concentration of heavy metals before adsorption, C_e (mg/L) is the equilibrium concentration of heavy metals, q_e (mg/g) is the amount of heavy metals adsorbed at equilibrium, m (g) is the mass of the composite used, and V (L) is the volume of heavy metal solution used.

The rate of adsorption can be affected by a myriad of factors in any given experiment. In this study, the effects of contact time, initial metal concentration, adsorbent mass, initial solution pH and temperature on the rate of adsorption were studied and described in detail in the following sections.

To assess the effect of solution pH on Cu^{2+}, Pb^{2+}, Cd^{2+} and Zn^{2+}ion adsorption onto the composite, the initial pH of the solutions from 2 to 12 was monitored. The adsorbate concentration was fixed at 10 mg/L with adsorbent dosage of 0.1 g, solution volume of 0.1 L and temperature of 298 K. The pH of the solution was adjusted by using 0.1 M hydrochloric acid or 0.1 M sodium hydroxide and was measured using a pH meter. The effect of pH solution on the adsorption percent removal of heavy metals onto AC-Ag-SO_2 nanocomposite is shown in Fig. 5a. The adsorption of Cu^{2+}, Pb^{2+}, Cd^{2+} and Zn^{2+} ions on AC-Ag-SO_2 composite was maximum at pH of 5.5 ± 0.5 and gradually decreased as the pH increased. This shows that at low pH, the number of hydrogen ions (H^+ ions) in the solution dominates and competes for chelation and complexation with metal ions on the adsorption sites [69]. However, at high pH, the hydroxide ions (OH^- ions) also dominates in the reaction medium and metal ions are more likely to precipitate in form of metal hydroxides [70]. Thus, too much competition between the hydrogen ions (H^+ ions) and hydroxide ions (OH^- ions) with metal ions would affect the percentage removal of heavy metals by the composite as shown in Fig. 5a.

The effect of contact time is significant in determining kinetic parameters and in approximating equilibrium time for the adsorption process. Influence of contact time on adsorption of Cu^{2+}, Pb^{2+}, Cd^{2+} and Zn^{2+} ions on the composite (AC-Ag-SO_2) was assessed by conducting adsorption experiments at different contact times ranging from 0 to 280 min and keeping other parameters constant. The percentage removal of Cu^{2+}, Pb^{2+}, Cd^{2+} and Zn^{2+} ions increased rapidly in the first 40 min and thereafter, increased gradually. With increase in contact time from 0 to 280 min, the percentage removal increased and reached a steady value of 94.3 ± 0.0068, 99.2 ± 0.0021, 90.2 ± 0.0102, 97.4 ± 0.0069% for Cu^{2+}, Pb^{2+}, Cd^{2+} and Zn^{2+} ions, respectively (Fig. 5b). This trend have been observed by ([104], [31,71,72]. The rate of adsorption increased rapidly in the first 40 min, then it proceeded gradually until equilibrium was established in approximately 200 min indicating that the adsorption sites were well exposed [71]. The increase in the rate of adsorption in the first 40 min can be attributed to high number of adsorption sites on the adsorbent at the beginning of the adsorption process. The effect of initial single metal ion concentration on the adsorption Cu^{2+}, Pb^{2+}, Cd^{2+} and Zn^{2+} ions onto AC-Ag-SiO_2 composite was investigated. The concentrations ranged from 10 mg/L to 100 mg/L and other parameters were kept constant (adsorbent dosage = 0.1 g, pH = 5.5, T = 298 K, $V_{solution}$ = 0.1 L and t = 200 min). From Fig. 5c, it was observed that, as the concentration of metal ions increased from 10 mg/L to 100 mg/L, the percentage removal decreased from 94.46 ± 0.0176 to 72.53 ±

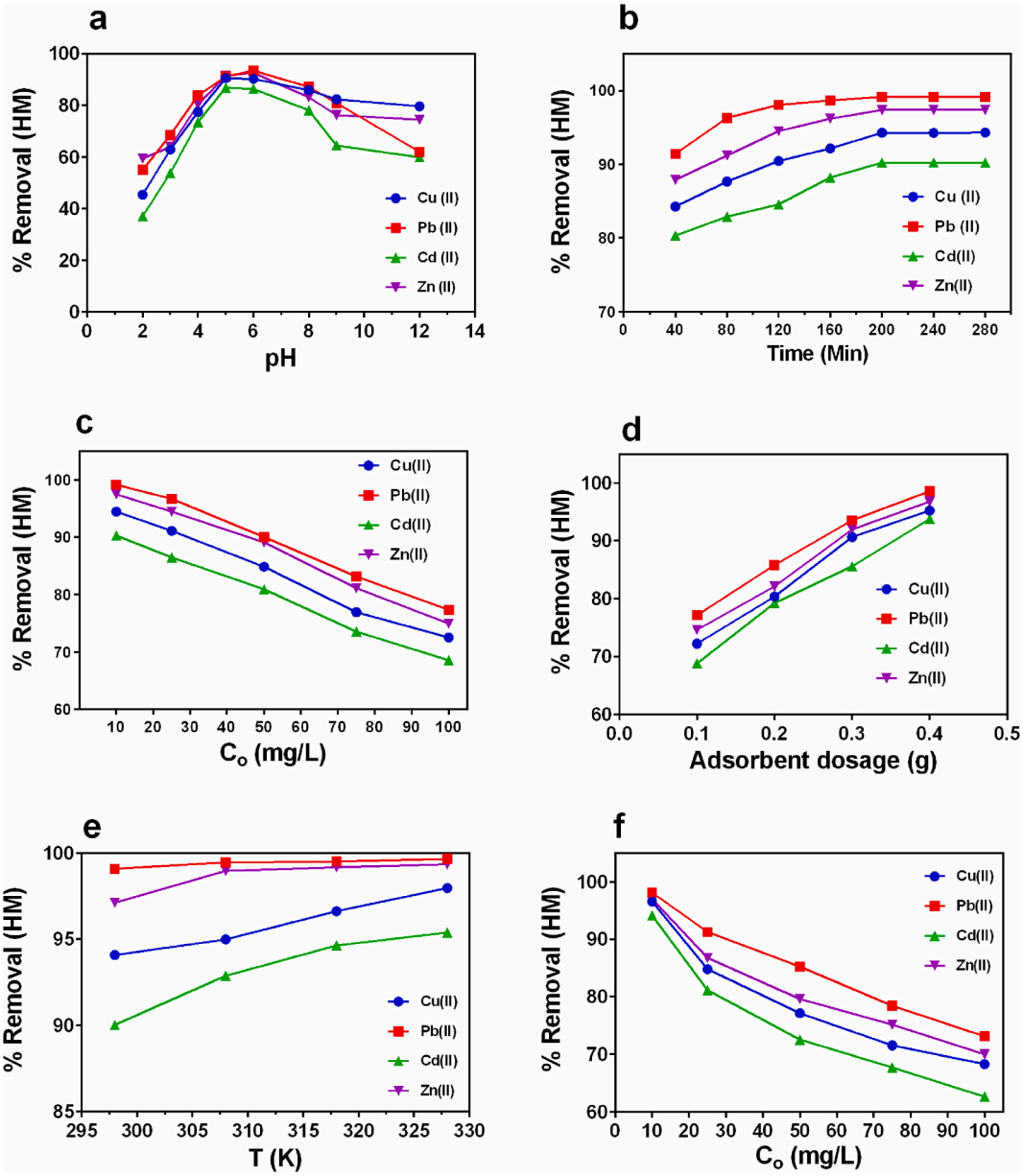

Fig. 5. Effect of (a) pH, (b) contact time, (c) initial metal ion concentration, (d) adsorbent dosage, (e) temperature and (f) multiple ion initial concentration on the percent removal of Cu^{2+}, Pb^{2+}, Cd^{2+} and Zn^{2+} ions on AC-Ag-SiO_2 composite (adsorbent dosage = 0.1 g, T = 298 K, $V_{solution}$ = 0.1 L, t = 200 min and initial metal concentration = 10 mg/L).

0.1097, 99.15 ± 0.0173 to 77.35 ± 0.2659, 90.3 ± 0.0353 to 68.57 ± 0.1655 and 97.49 ± 0.0115 to 74.97 ± 0.1784 for Cu^{2+}, Pb^{2+}, Cd^{2+} and Zn^{2+} ions, respectively. The decrease in percentage removal as metal ion concentration increased could be attributed to a high number of metal ions in the solution compared to the available sites of adsorption on the surface of the adsorbent [71,73]. It is evident from the results obtained that the adsorption of metal ions onto AC-Ag-SiO_2 composite was dependent on the initial metal concentration.

The effect of adsorbent dosage (AC-Ag-SiO_2 composite) on the removal of Cu^{2+}, Pb^{2+}, Cd^{2+} and Zn^{2+} ions at constant concentration (75 mg/L) were investigated by agitating with different adsorbent dosage over the range of 0.1 g–0.4 g. From Fig. 5d, it can be observed that increasing the adsorbent dosage resulted in an increase in percentage removal of metal ions. The increase in percentage removal as the adsorbent dosage increased can be attributed to the availability of more active adsorption sites on the surface of the adsorbent.

Temperature is an important parameter that affects the adsorption of heavy metals on an adsorbent. The effect of temperature on the adsorption of heavy metal ions onto AC-Ag-SiO_2 composite was studied in the temperature range of 298 K–328 K and other parameters were kept constant (adsorbent dosage = 0.1 g, pH = 5.5, $V_{solution}$ = 0.1 L, initial metal ion concentration = 10 mg/L and t = 200 min). The result obtained showed that increasing solution temperature increased the percentage removal of heavy metals (Fig. 5e). Higher temperatures favour metal ion mobility to penetrate inside the adsorbent pores due to increased energy [74]. Furthermore, when the temperature increases, there is an increased diffusion of metal ions across the external and boundary layer and the internal pores of the adsorbent [75].

3.2.1. *Study of simultaneous removal of multiple metal ions*

The composite was also evaluated for simultaneous removal of multiple metal ions from aqueous solution. The aqueous solutions contained equal amounts of Cu^{2+}, Pb^{2+}, Cd^{2+} and Zn^{2+} ions, respectively (Fig. 5f). As the concentration increased from 10 mg/L to 100 mg/L the

percentage removal decreased from 96.60 ± 0.2085 to 68.30 ± 1.8626, 98.14 ± 0.4370 to 73.13 ± 0.4383, 94.17 ± 0.1660 to 62.64 ± 0.4092 and 97.01 ± 0.1299 to 70.01 ± 0.5605 for Cu^{2+}, Pb^{2+}, Cd^{2+} and Zn^{2+} ions, respectively.

3.3. Adsorption isotherms

3.3.1. Langmuir adsorption isotherm

The isotherm explains that monolayer adsorption of the adsorbate takes place on an evenly distributed surface of the adsorbent [28]. The sites of adsorption have equal affinity for adsorption and the interaction of adsorbed molecules is restricted [42]. The isotherm for single solute adsorption can be represented as follows ([99] [41],:

$$q_e = \frac{1}{q_m K_L} + \frac{C_e}{q_m} \quad (3)$$

The linear equation is written as [76]:

$$\frac{C_e}{q_e} = \frac{1}{K_L q_m} + \frac{C_e}{q_m} \quad (4)$$

where q_e (mg/g) is the amount of heavy metals adsorbed at equilibrium, C_e (mg/L) is the equilibrium concentration of heavy metals, q_m (mg/g) is the maximum adsorption capacity and K_L (L/mg) is the Langmuir constant which measures the affinity of metal ions towards the adsorbent adsorption sites. Thus, the magnitude of K_L indicates either a strong or weak interaction between the heavy metal ions and the adsorption sites of the adsorbent. The parameters q_m and K_L were determined from the plot of $\frac{C_e}{q_e}$ versus C_e [77]. The separation factor, R_L, was determined from the equation below [78]; [100], [42];

$$R_L = \frac{1}{1 + K_L C_o} \quad (5)$$

where R_L is the separation factor, C_o (mg/L) is the concentration of heavy metals before adsorption and K_L is the Langmuir constant. The value of the separation factor indicates the favorability of the adsorption process [42,79].

The parameters of Langmuir isotherm i.e., q_m, K_L and R_L for heavy metal ions using AC-Ag-SiO_2 were obtained from the plot of C_e/q_e versus C_e as shown in Fig. 6a and are shown in Table 1. The maximum adsorption capacity for AC-Ag-SiO2 composite was found to be 84.75 ± 0.242, 81.3 ± 0.197, 87.72 ± 0.961 and 81.97 ± 0.389 mg/g for the removal of Cu^{2+}, Pb^{2+}, Cd^{2+} and Zn^{2+} ions, respectively. The R^2 for the isotherm were 0.9786, 0.9742, 0.9873 and 0.9836 for Cu^{2+}, Pb^{2+}, Cd^{2+} and Zn^{2+} ions, respectively. The estimated values of R_L ranged between 0.02 ± 0.006 and 0.50 ± 0.002 for all the heavy metals, which indicates

Table 1
Adsorption isotherm models parameters of Cu^{2+}, Pb^{2+}, Cd^{2+} and Zn^{2+} ions adsorption by AC-Ag-SiO_2 composite.

Isotherm models	Parameters	Cu^{2+}	Pb^{2+}	Cd^{2+}	Zn^{2+}
Langmuir model	q_m (mg/g)	84.75 ± 0.24	81.3 ± 0.2	87.72 ± 0.96	81.97 ± 0.39
	K_L (L/mg)	0.16 ± 0.004	0.44 ± 0.07	0.1 ± 0.03	0.29 ± 0.004
	R_L	0.06 ± 0.006 to 0.38 ± 0.001	0.02 ± 0.006 to 0.19 ± 0.001	0.09 ± 0.01 to 0.50 ± 0.002	0.03 ± 0.003 to 0.25 ± 0.0004
	R^2	0.9786	0.9742	0.9873	0.9836
Freundlich model	K_F (mg/g)	13.839 ± 0.19	24.95 ± 0.3	9.92 ± 0.12	19.22 ± 0.104
	n_F (g/L)	1.943 ± 0.01	2.737 ± 0.352	1.721 ± 0.151	2.26 ± 0.232
	R^2	0.9911	0.9992	0.9905	0.9922
Temkin model	b_T	157.02 ± 0.39	211.78 ± 0.98	145.95 ± 0.74	176.24 ± 1.571
	K_T	2.52 ± 0.06	16.94 ± 0.86	1.377 ± 0.024	5.70 ± 0.05
	R^2	0.9657	0.9387	0.9702	0.9669

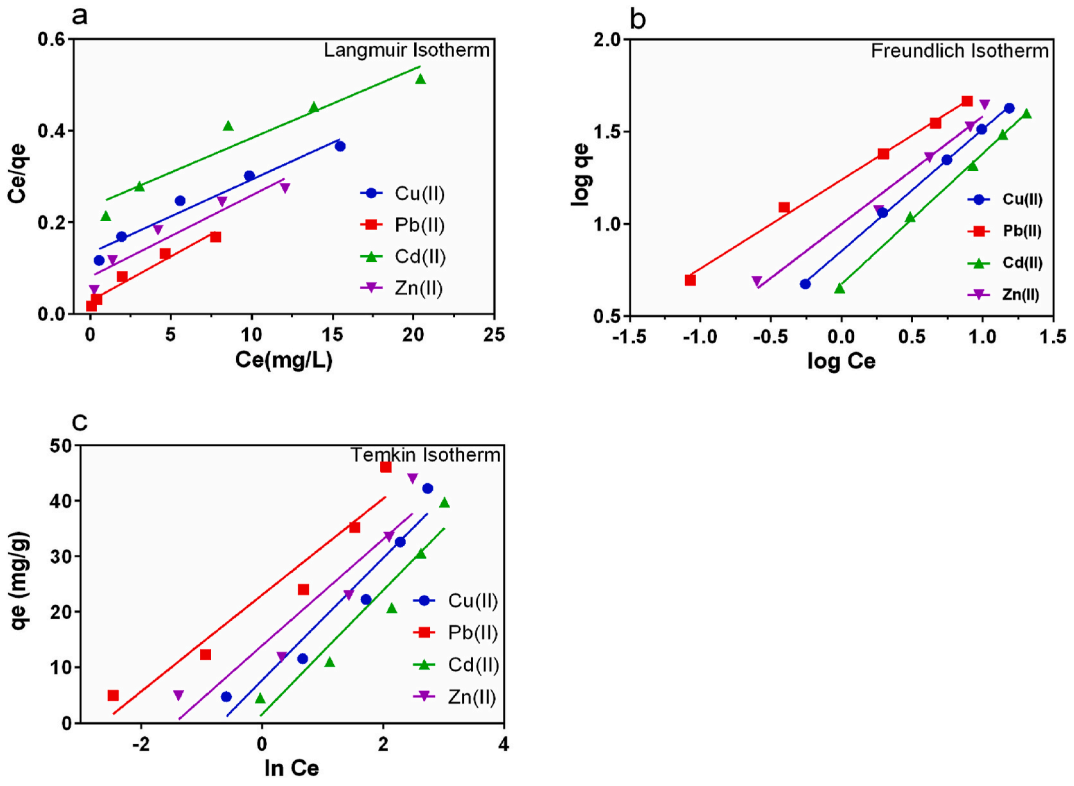

Fig. 6. (a) Langmuir, (b) Freundlich and (c) Temkin adsorption isotherm for Cu^{2+}, Pb^{2+}, Cd^{2+} and Zn^{2+} ions adsorption onto AC-Ag-SiO_2 composite.

favorable adsorption. The values of K_L ranging between 0.099 ± 0.003 and 0.436 ± 0.017 for all the heavy metals shows that the interaction of metals with the composite was not strong.

3.3.2. Freundlich isotherm

Unlike the Langmuir adsorption isotherm, Freundlich isotherm assumes that the adsorbent sites have different binding energy for adsorption of metal ions [101]. The isotherm is described by equation (6) [80];

$$q_e = K_e C_e^{\frac{1}{n}} \quad (6)$$

Equation (6) can be written in logarithmic form for the linearization of experimental data. The equation is given by Ref. [81]:

$$\log\ q_e = (\log\ C_e)/n + \log\ K_F \quad (7)$$

where q_e (mg/g) is the amount of heavy metals adsorbed at equilibrium, C_e (mg/L) is the equilibrium concentration and K_F is the Freundlich constant and n is the adsorption intensity. The value of n is very useful in differentiating a physical adsorption from chemical adsorption process ([103], [73]. The values K_F and n were calculated from the slope and intercept of the plot of log q_e versus log C_e.

The Freundlich isotherm parameters K_F and n_F (Table 1) were calculated from the slope and intercept of the linearized plot of ln q_e versus ln C_e (Fig. 6b). The values of n_F is found as 1.943 ± 0.012, 2.737 ± 0.352, 1.721 ± 0.151 and 2.258 ± 0.232 for adsorption of Cu^{2+}, Pb^{2+}, Cd^{2+} and Zn^{2+} ions, respectively. The obtained values of n_F are greater than 1 and as such, physiosorption phenomena during metal adsorption onto AC-Ag-SiO_2 composite is supported [101]. The Freundlich regression correlation coefficient (R^2) values were 0.9911, 0.9992, 0.9905 and 0.9922 for Cu^{2+}, Pb^{2+}, Cd^{2+} and Zn^{2+} ions, respectively. The R^2 values for Freundlich isotherm model were greater in comparison with the other two isotherms.

3.3.3. Temkin isotherm

The Temkin isotherm studies the indirect effect of the interaction of the adsorbate and the adsorbent during the process of adsorption. The isotherm provides valuable information on the binding energy and the heat of adsorption [82]. The binding energies are evenly distributed during the adsorption process. The isotherm is best described by the equation below [28,68,83]:

$$q_e = \frac{RT}{b} \ln K_T + \frac{RT}{b} \ln C_e \quad (8)$$

where K_T is the Temkin isotherm constant (L/mol), b is a constant related to the adsorption heat, R is the gas constant (8.314 $JK^{-1}mol^{-1}$) and T is the temperature at 298 K [68].

The Temkin adsorption parameters b_T and K_T were calculated from the plot of q_e (mg/g) versus *In* C_e (Fig. 6c) and are tabulated in the first table (Table 1). The R^2 values obtained for Temkin isotherm model was 0.9657, 0.9387, 0.9702 and 0.9669 for Cu^{2+}, Pb^{2+}, Cd^{2+} and Zn^{2+} ions. In comparison to Langmuir and Freundlich adsorption model the R^2 of Temkin isotherm were small. Thus, the isotherm could not be used to design the adsorption process; rather it was used to compare the behavior of equilibrium experiments to that of the Freundlich and Langmuir adsorption models.

Therefore, a comparison of the regression correlation coefficient (R^2) values for Langmuir, Freundlich and Temkin isotherm model for removal of heavy metal ions onto AC-Ag-SiO_2 composite shows that the equilibrium data is best fitted with the Freundlich isotherm model. Thus, multi-layer and heterogeneous adsorption of metal ions on AC-Ag-SiO_2 composite surface is supported.

3.4. Adsorption kinetics

The pseudo-first order and pseudo-second order kinetic models were evaluated to understand the kinetic mechanism that controls the adsorption process for the removal of heavy metal ions on AC-Ag-SiO_2 composite. The calculated parameters for the kinetic models are tabulated in Table 2.

3.4.1. Pseudo-first order kinetic model

The parameters of pseudo-first-order kinetic model can be calculated from equations below [76,77].

$$\log(q_e - q_t) = \log q_e - K_1 \frac{t}{2.303} \quad (9)$$

where q_e and q_t are the amounts of heavy metals adsorbed at equilibrium and at time t (minute), respectively.

The model materiality was typically assessed by plotting the graph of $log(q_e - q_t)$ versus t which gives the slope of K_1 and intercept of $log q_e$. If the parameter $log q_e$ is not equal to the intercept of plot of $\log(q_e - q_t)$ versus t then the adsorption is not likely to follow a first-order- kinetic pathway regardless of the high coefficient of determination [72,84–86].

The model parameters (Table 2) were obtained from the plot of $\log(q_e - q_t)$ versus t (Fig. 7a). The R^2 values for the model were 0.9891, 0.9977, 0.8207 and 0.9664 for Cu^{2+}, Pb^{2+}, Cd^{2+} and Zn^{2+} ions, respectively. The calculated values of the adsorption capacity (q_e *cal*) for pseudo-first- order kinetic model were 1.7762 ± 0.029, 1.8795 ± 0.039, 1.9063 ± 0.058 and 2.1774 ± 0.095 for Cu^{2+}, Pb^{2+}, Cd^{2+} and Zn^{2+} ions, respectively. The values above for q_e *cal* are not in good agreement with the experimental adsorption capacities (q_e *exp*) of heavy metal ions.

3.4.2. Pseudo-second order kinetic model

The model can be expressed as [78,87]:

$$\frac{t}{q_t} = \frac{1}{K_2 q_e^2} + \frac{1}{q_e} t \quad (10)$$

where, K_2 (g/mg.h) is the rate constant of second-order adsorption.

The kinetic parameters for the model q_e *cal* and K_2 (Table 2) were obtained from the slope $\left(\frac{1}{q_e}\right)$ and intercept $\left(\frac{1}{K_2 q_e^2}\right)$ of the linear plot of $\frac{t}{q_t}$ versus t (Fig. 7b). The regression correlation coefficient (R^2) values for the model were 0.9999, 0.999999, 0.9997 and 0.99995 for Cu^{2+}, Pb^{2+}, Cd^{2+} and Zn^{2+} ions. The calculated values of the adsorption capacity (q_e *cal*) for pseudo-second order kinetic model were 9.703 ± 0.0048, 10.061 ± 0.0056, 9.332 ± 0.0126 and 9.981 ± 0.0071 for Cu^{2+}, Pb^{2+}, Cd^{2+} and Zn^{2+} ions, respectively. The values above for q_e *cal* are in good agreement with the experimental adsorption capacities (q_e *exp*) for the heavy metal ions. The values of K_2 for all the metals are less than 1 which indicates that adsorption was high in the initial stage and

Table 2
Adsorption kinetics models parameters of Cu^{2+}, Pb^{2+}, Cd^{2+} and Zn^{2+} ions adsorption by AC-Ag-SiO2 nanocomposite.

Kinetic model	parameters	Metal			
		Cu^{2+}	Pb^{2+}	Cd^{2+}	Zn^{2+}
Pseudo-1st-order kinetics	q_e *exp* (mg/g)	9.43 ± 0.01	9.92 ± 0.002	9.02 ± 0.01	9.74 ± 0.01
	R^2	0.9891	0.9977	0.8207	0.9664
	q_e *cal* (mg/g)	1.78 ± 0.03	1.88 ± 0.04	1.91 ± 0.06	2.18 ± 0.1
	K_1	0.013 ± 0.0004	0.02 ± 0.0002	0.013 ± 0.001	0.02 ± 0.001
Pseudo-2nd-order kinetics	R^2	0.9999	0.999999	0.9997	0.99995
	q_e *cal* (mg/g)	9.70 ± 0.005	10.1 ± 0.01	9.33 ± 0.013	9.98 ± 0.01
	K_2	0.014 ± 0.0002	0.03 ± 0.001	0.012 ± 0.001	0.02 ± 0.001

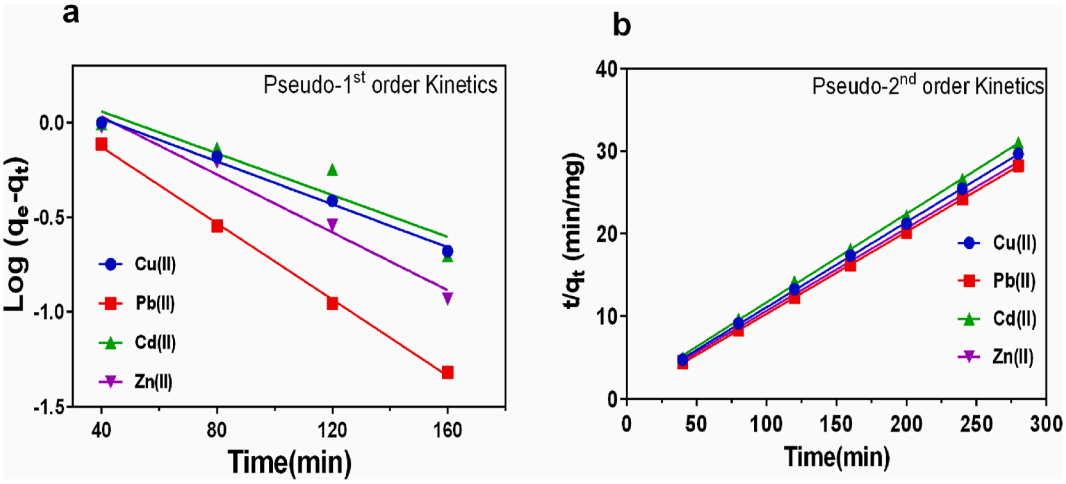

Fig. 7. (a) pseudo-first-order and (b) pseudo-second-order kinetics for Cu^{2+}, Pb^{2+}, Cd^{2+} and Zn^{2+} ions adsorption onto AC-Ag-SiO_2 composite.

decreased with lapse in time [72].

A comparison of the correlation coefficients and the equilibrium adsorption capacities of the two models show that pseudo-second-order kinetic model possesses higher correlation coefficients and has calculated equilibrium capacities that are close to the experimental equilibrium capacities for all the metal ions. The adsorption kinetic data suitably described pseudo-second-order kinetic model.

3.5. Thermodynamic studies

The change in Gibbs free energy (ΔG°) was calculated using equations below [73,88]; [102]);

$$K_C = \frac{q_e}{C_e} \tag{11}$$

$$\Delta G^\circ = -RTInK_C \tag{12}$$

$$\Delta G^\circ = \Delta H^\circ - T\Delta S^\circ \tag{13}$$

The enthalpy change (ΔH°) and entropy change (ΔS^o) change was determined from the Van't Hoff equation below [31,89].

$$InK = \frac{-\Delta H^\circ}{RT} + \frac{\Delta S^\circ}{R} \tag{14}$$

Therefore,

$$\Delta H^\circ = -R \times Slope \tag{15}$$

$$\Delta S = R \times Intercept \tag{16}$$

where T is the absolute temperature (K), ΔG^o ($kJ.mol^{-1}$) is the Gibbs free energy change, ΔH^o ($kJ.mol^{-1}$) is the enthalpy change, R is gas constant (8.314 $Jmol^{-1}K^{-1}$) and ΔS^o ($kJmol^{-1}K^{-1}$) is the entropy change.

A thermodynamic analysis of adsorption process of heavy metal ions on the composite was carried out to evaluate and estimate the practicality of the adsorption process. The Gibbs free energy change (ΔG°), enthalpy change (ΔH°) and entropy change (ΔS°), are presented in Table 3; the Gibbs free energy change at temperatures from 298 K to 328 K for adsorption of the metal ions were all negative showing the feasibility and the spontaneous nature of the adsorption process ([100], [101]). It was also observed that as the temperature was increased, the change in free energy increased gradually. This is largely because of the activation of more sites on the surface of the adsorbent as the temperature increases [90]. For physical adsorption the free energy change (ΔG°) ranges between (−20 and 0) kJ/mol and for chemical adsorption it ranges between (−80 and −400) kJ/mol [29,79,90]. The free energy change for all metal ions ranged between (−5.4493 and −15.572) kJ/mol which means physical adsorption was more predominant.

Table 3
Thermodynamic parameters for Cu^{2+}, Pb^{2+}, Cd^{2+} and Zn^{2+} ions adsorption onto AC-Ag-SiO_2 composite.

Metal	T (K)	K_C	ΔG (kJ/mol)	ΔH (kJ/mol)	ΔS (J/K.mol)
Cu^{2+}	298	15.89 ± 1.31	−6.85 ± 0.19	30.24 ± 4.79	123.6 ± 16.02
	308	18.96 ± 1.76	−7.53 ± 0.23		
	318	28.67 ± 2.74	−8.87 ± 0.24		
	328	48.26 ± 9.76	−10.57 ± 0.54		
Pb^{2+}	298	108.89 ± 3.80	−11.62 ± 0.09	25.89 ± 1.74	126.4 ± 6.15
	308	184.19 ± 16.76	−13.36 ± 0.24		
	318	207.33 ± 20.91	−14.10 ± 0.26		
	328	302.03 ± 31.11	−15.57 ± 0.27		
Cd^{2+}	298	9.02 ± 1.35	−5.45 ± 0.35	22.81 ± 4.50	95.1 ± 14.33
	308	13.03 ± 1.19	−6.57 ± 0.23		
	318	17.66 ± 1.10	−7.59 ± 0.17		
	328	20.69 ± 2.05	−8.26 ± 0.281		
Zn^{2+}	298	33.72 ± 3.62	−8.72 ± 0.99	39.12 ± 8.70	162.4 ± 27.17
	308	96.09 ± 5.28	−11.69 ± 0.74		
	318	120.95 ± 12.54	−12.68 ± 0.26		
	328	152.85 ± 11.13	−13.72 ± 0.20		

The values of the enthalpy change (ΔH°) and entropy change (ΔS^o) change were determined from the slope and intercept of the Van't Hoff plot (Fig. 8). The changes in enthalpy (ΔH°) were 30.24 ± 4.794, 25.89 ± 1.744, 22.81 ± 4.499 and 39.12 ± 8.702 kJ/mol for adsorption of Cu^{2+}, Pb^{2+}, Cd^{2+} and Zn^{2+} ions; showing the endothermic nature of the adsorption process. The change in entropy (ΔS°) was also evaluated and the values of ΔS° were 123.6 ± 6.146, 126.4 ± 6.146, 95.1 ± 14.325 and 162.4 ± 27.168 J/mol K for Cu^{2+}, Pb^{2+}, Cd^{2+} and Zn^{2+} ions, respectively. The positive values of entropy (ΔS°) show that there is an increased disorder in the interaction of metal ions with the composites surface as adsorption progresses.

3.6. Regeneration studies

The regeneration of an adsorbent is very significant as it makes the

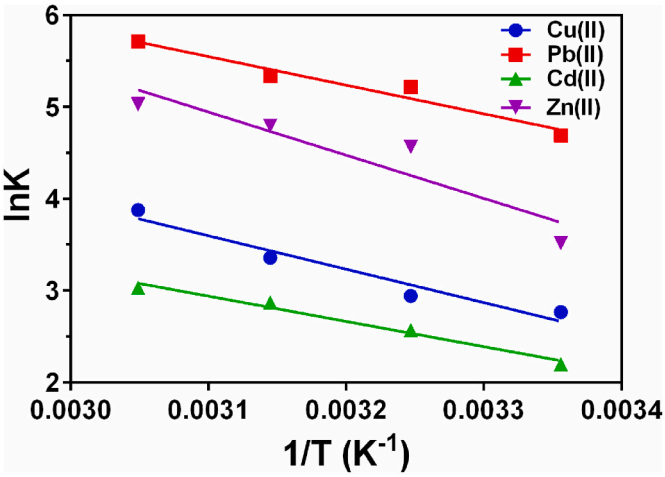

Fig. 8. Van't Hoff plot for the adsorption of Cu^{2+}, Pb^{2+}, Cd^{2+} and Zn^{2+} ions onto AC-Ag-SiO_2 composite.

adsorption process more economical and reduces the environmental impact [91]. In this study, the utilized AC-Ag-SiO_2 composite was treated with 1 M sodium hydroxide for 24 h followed by 24 h treatment with 1 M HCI for desorption of heavy metal ions on the adsorbent [72]. Regeneration experiments were performed by dispersing 0.4 g of the regenerated adsorbent into 100 ml of 10, 25, 50, 75 and 100 mg/L multi-component solutions containing Cu^{2+}, Pb^{2+}, Cd^{2+} and Zn^{2+} ions and agitated at 250 rpm at a temperature of 298 K for 200 min. Two recycles were achieved by repeating the same procedure. Analysis of variance executed in Excel 2016 for a single factor showed that there was no statistically significant difference between the initial and two cycle regeneration-adsorption ($p > 0.9$). The result confirms that the composite can be reused with effective removal efficiency of heavy metal ions as shown Fig. 9 a-d. In all the cases, percent removal was more than 60% for the highest concentration at 100 mg/L metal ion.

3.7. Comparison of adsorption capacity of various adsorbents with the present study

The adsorption capacity for the activated carbon silver-silica composite was compared with other sorption materials. Table 4 shows the adsorption capacity for single metal ions; copper, lead cadmium and zinc respectively.

3.8. Proposed mechanism of adsorption

The carbon in the composite was activated by sulphuric acid followed by thermal treatment which developed the acidic oxides on its surface [72]. Thus, the suggested adsorption mechanism is ion exchange

Table 4
Comparison of adsorption capacities for the removal of Cu^{2+}, Pb^{2+}, Cd^{2+} and Zn^{2+} ions with various adsorbents.

Adsorbent	q_e (mg/g)				References
	Cu^{2+}	Pb^{2+}	Cd^{2+}	Zn^{2+}	
AC-Ag-SiO_2	84.75 ± 0.24	81.30 ± 0.2	87.72 ± 0.96	81.97 ± 0.24	**This work**
WSA/Starch/Fe_3O_4	45.4	–	–	–	[102]
ACL/Fe_3O_4	–	–	39.6	–	[92]
Nano-silica	–	–	53.13	–	[21]
Eggshell/starch/Fe_3O_4	–	57.14	48.54	–	[93]
BPB/Fe_3O_4/ZIF-67	–	–	50.78	–	[102]
nANB	21.23	26.32	20.83	11.90	[72]
AC/$NiFe_2O_4$	105.8	–	–	75.1	[94]

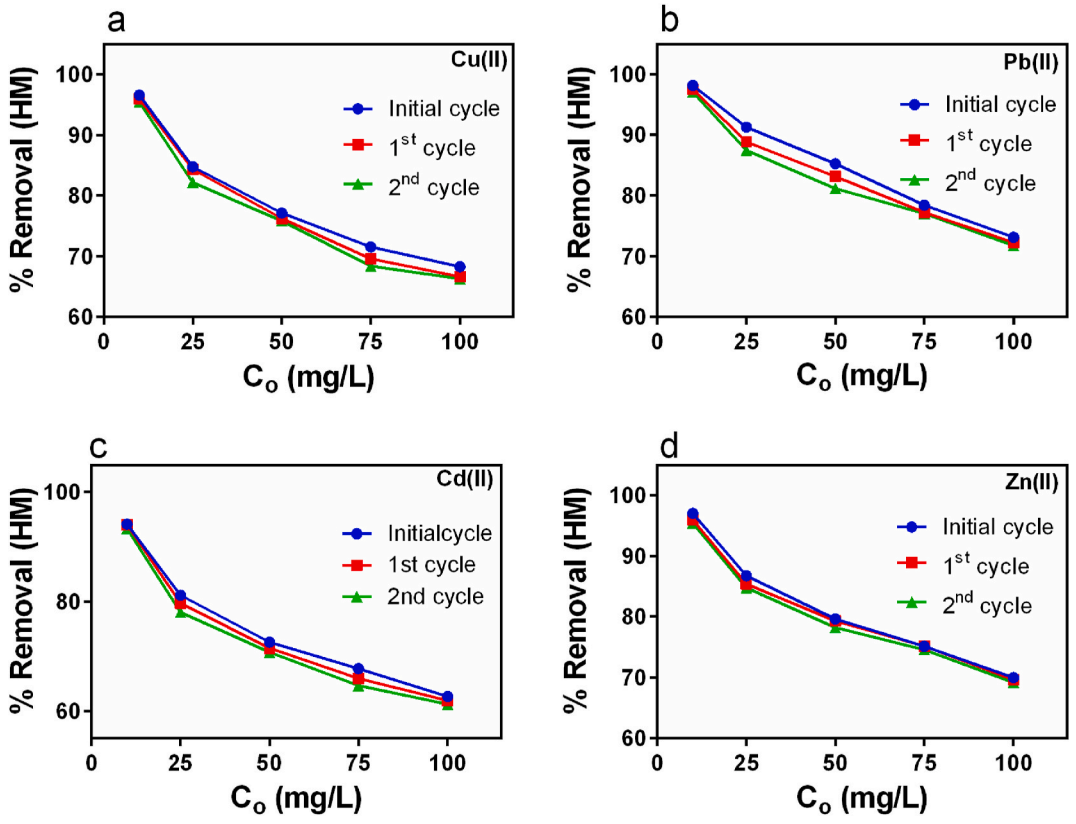

Fig. 9. Percentage removal of (a) Cu^{2+}, (b) Pb^{2+}, (c) Cd^{2+} and (d) Zn^{2+} by regenerated AC-Ag-SiO_2 composite.

which is based on the model of metal binding and proton releasing reaction [95] of Cu^{2+}, Pb^{2+}, Cd^{2+} and Zn^{2+} ions on AC-Ag-SiO_2 composite. Furthermore, in aqueous medium, the silica surface forms silanol groups (e.g. –Si(OH), -$Si(OH)_2$, -$Si(OH)_3$) at the interface [96]. In principle, adsorption through electrostatic interactions between dissolved cations and negatively charged silanolate surface site can occur. Nevertheless, experimental evidence suggests ion exchange as the primary adsorption mechanism [69,96].

4. Conclusion

In this study, activated carbon, silver nanoparticles (Ag NPs), silica nanoparticles (SiO_2 NPs) and activated carbon-supported silver and silica nanoparticles composite (AC-Ag-SiO_2) were successfully synthesized. The prepared materials were characterized using Fourier Transform Infrared spectroscopy (FT-IR), Ultraviolet–visible spectroscopy (UV–Vis), Atomic Force Microscopy (AFM) and X-Ray Diffraction (XRD). The composite (AC-Ag-SiO_2) was also assessed for adsorption of Cu (Hamwiinga et al.), Pb (Hamwiinga et al.), Cd (Hamwiinga et al.) and Zn (Hamwiinga et al.) ions from water. Batch adsorption experiments were conducted to study the influence of several factors such as pH, adsorbent dose, contact time, temperature and initial metal ion concentration on adsorption of Cu^{2+}, Pb^{2+}, Cd^{2+} and Zn^{2+} ions. The adsorbent was able to remove metal ions individually and as a multi-ion mixture. The Freundlich isotherm model and pseudo-second-order kinetic model provided a better fit to the experimental data. The maximum adsorption capacity was found to be 84.75 ± 0.24, 81.30 ± 0.2, 87.72 ± 0.96 and 81.97 ± 0.39 mg/g for Cu^{2+}, Pb^{2+}, Cd^{2+} and Zn^{2+} ions, respectively. The obtained values of thermodynamic parameters such as Gibbs energy (ΔG°), enthalpy (ΔH°), and entropy (ΔS°) showed that the adsorption process of Cu^{2+}, Pb^{2+}, Cd^{2+} and Zn^{2+} ions onto AC-Ag-SiO_2 composite was spontaneous, feasible, endothermic and physical in nature. Regeneration studies revealed that AC-Ag-SiO_2 composite could be reused effectively.

Funding

The student tuition was partially funded by the International Programme in Chemical Sciences (IPICS) under the Material Science and Plant Natural Products project grants ZM01 and ZM02 respectively.

Author credit statement

JN conceptualized the research and designed experiments, GK and JN, collected plant samples, GK executed the experiments. JN and OM supervised the works. JN drafted the paper. OM and GK reviewed the manuscript. All authors proofread and agreed to co-publish the manuscript.

Declaration of competing interest

The authors declare that they have no known competing financial interests or personal relationships that could have appeared to influence the work reported in this paper.

Acknowledgements

The authors would like to thank members of the Departments of Chemistry and Physics, School of Natural Sciences, Department of Mines and International Science Program (ISP) through support from the Plant Natural Products Research and Material Sciences Research Groups.

References

[1] R. Singh, R. Bhadouria, P. Singh, A. Kumar, S. Pandey, V.K. Singh, Nanofiltration technology for removal of pathogens present in drinking water, in: Waterborne Pathogens, Elsevier, 2020, pp. 463–489.
[2] N. Tara, S.I. Siddiqui, G. Rathi, S.A. Chaudhry, A.M. Asiri, Nano-engineered adsorbent for the removal of dyes from water: a review, Curr. Anal. Chem. 16 (1) (2020) 14–40.
[3] D. Boehm, A. Lecus, H.-F. Zhang, D. Garman, M.R. Silva, Removal of emerging persistent organic pollutants (Em-POPs) model compounds from water using a natural porous material functionalized with graphene-based products, h2oj 3 (1) (2020) 416–427.
[4] J. Nyirenda, A. Mwanza, C. Lengwe, Assessing the biodegradability of common pharmaceutical products (PPs) on the Zambian market, Heliyon 6 (10) (2020), e05286.
[5] F. Hamwiinga, C.D. Meki, P. Mubita, H. Halwiindi, Heavy metal levels in drinking water sources of Chingola District, Zambia, 2020.
[6] S. Dytłow, B. Górka-Kostrubiec, Concentration of heavy metals in street dust: an implication of using different geochemical background data in estimating the level of heavy metal pollution, Environ. Geochem. Health 43 (1) (2021) 521–535.
[7] J. Vidal, Zambian Villagers Take Mining Giant Vedanta to Court in UK over Toxic Leaks, vol. 1, The Guardian, 2015.
[8] A.A. Al-Taani, Y. Nazzal, F.M. Howari, J. Iqbal, N. Bou Orm, C.M. Xavier, A. Bărbulescu, M. Sharma, C.-S. Dumitriu, Contamination assessment of heavy metals in agricultural soil, in the Liwa area (UAE), Toxics 9 (3) (2021) 53.
[9] N. Wang, Y. Qiu, K. Hu, C. Huang, J. Xiang, H. Li, J. Tang, J. Wang, T. Xiao, One-step synthesis of cake-like biosorbents from plant biomass for the effective removal and recovery heavy metals: effect of plant species and roles of xanthation, Chemosphere 266 (2021), 129129.
[10] G.K.R. Angaru, Y.-L. Choi, L.P. Lingamdinne, J.-S. Choi, D.-S. Kim, J.R. Koduru, J.-K. Yang, Y.-Y. Chang, Facile synthesis of economical feasible fly ash–based zeolite–supported nano zerovalent iron and nickel bimetallic composite for the potential removal of heavy metals from industrial effluents, Chemosphere 267 (2021), 128889.
[11] U.T. Pettersson, J. Ingri, The geochemistry of Co and Cu in the Kafue River as it drains the Copperbelt mining area, Zambia, Chem. Geol. 177 (3–4) (2001) 399–414.
[12] K. Choongo, M. Syakalima, M. Mwase, Coefficient of condition in relation to copper levels in muscle of serranochromis fish and sediment from the Kafue river, Zambia, Bull. Environ. Contam. Toxicol. 75 (4) (2005) 645–651.
[13] B.D. Tembo, K. Sichilongo, J. Cernak, Distribution of copper, lead, cadmium and zinc concentrations in soils around Kabwe town in Zambia, Chemosphere 63 (3) (2006) 497–501.
[14] Y. Ikenaka, S.M. Nakayama, K. Muzandu, K. Choongo, H. Teraoka, N. Mizuno, M. Ishizuka, Heavy metal contamination of soil and sediment in Zambia, Afr. J. Environ. Sci. Technol. 4 (11) (2010) 729–739.
[15] M.N. Chileshe, S. Syampungani, E.S. Festin, M. Tigabu, A. Daneshvar, P.C. Odén, Physico-chemical characteristics and heavy metal concentrations of copper mine wastes in Zambia: implications for pollution risk and restoration, J. For. Res. (2019) 1–11.
[16] M.S. Kambole, Managing the water quality of the Kafue river, Phys. Chem. Earth, Parts A/B/C 28 (20–27) (2003) 1105–1109.
[17] M. Karnib, A. Kabbani, H. Holail, Z. Olama, Heavy metals removal using activated carbon, silica and silica activated carbon composite, Energy Proc. 50 (2014) 113–120.
[18] A.R. Contreras Rodríguez, Removal of Cadmium (II), Lead (II) and Chromium (VI) in Water with Nanomaterials, Universitat Autònoma de Barcelona, 2015.
[19] G. Mbewe, M. Mutondo, K. Maseka, K. Sichilongo, Assessment of heavy-metal pollution in sediments and tilapia fish species in Kafue River of Zambia, Arch. Environ. Contam. Toxicol. 71 (3) (2016) 383–393.
[20] G.A. Engwa, P.U. Ferdinand, F.N. Nwalo, M.N. Unachukwu, Mechanism and Health Effects of Heavy Metal Toxicity in Humans. Poisoning in the Modern World-New Tricks for an Old Dog? IntechOpen, 2019.
[21] R. Foroutan, R. Mohammadi, S.J. Peighambardoust, S. Jalali, B. Ramavandi, Application of nano-silica particles generated from offshore white sandstone for cadmium ions elimination from aqueous media, Environ. Technol. Innovat. 19 (2020), 101031.
[22] E.C. de Souza, A.S. Pimenta, A.J.F. da Silva, P.F.P. do Nascimento, J.O. Ighalo, Oxidized eucalyptus charcoal: a renewable biosorbent for removing heavy metals from aqueous solutions, Biomass Conv. Biorefinery (2021) 1–15.
[23] S. Wu, P. Yan, W. Yang, J. Zhou, H. Wang, L. Che, P. Zhu, ZnCl2 enabled synthesis of activated carbons from ion-exchange resin for efficient removal of Cu2+ ions from water via capacitive deionization, Chemosphere 264 (2021), 128557.
[24] S. Gunatilake, Methods of removing heavy metals from industrial wastewater, Methods 1 (1) (2015) 14.
[25] Z. Esvandi, R. Foroutan, S.J. Peighambardoust, A. Akbari, B. Ramavandi, Uptake of anionic and cationic dyes from water using natural clay and clay/starch/MnFe2O4 magnetic nanocomposite, Surface. Interfac. 21 (2020), 100754.
[26] S. Ganesan, Waste fruit cortexes for the removal of heavy metals from water, in: Green Adsorbents to Remove Metals, Dyes and Boron from Polluted Water, Springer, 2021, pp. 323–350.
[27] M. Gubari, Z. Ahmed, N. Alekseeva, Application of reverse osmosis in industrial wastewater desalination: systematic progress and its challenges, Наука в XXI веке: инновационный потенциал развития (2021).
[28] M.S. Abdelbassit, K.R. Alhooshani, T.A. Saleh, Silica nanoparticles loaded on activated carbon for simultaneous removal of dichloromethane,

trichloromethane, and carbon tetrachloride, Adv. Powder Technol. 27 (4) (2016) 1719–1729.
[29] A.M. Alkherraz, A.K. Ali, K.M. Elsherif, Removal of Pb (II), Zn (II), Cu (II) and Cd (II) from aqueous solutions by adsorption onto olive branches activated carbon: equilibrium and thermodynamic studies, Chem. Int. 6 (1) (2020) 11–20.
[30] V. Nejadshafiee, M.R. Islami, Intelligent-activated carbon prepared from pistachio shells precursor for effective adsorption of heavy metals from industrial waste of copper mine, Environ. Sci. Pollut. Control Ser. 27 (2) (2020) 1625–1639.
[31] R.S. El-Tawil, S.T. El-Wakeel, A.E. Abdel-Ghany, H.A. Abuzeid, K.A. Selim, A. M. Hashem, Silver/quartz nanocomposite as an adsorbent for removal of mercury (II) ions from aqueous solutions, Heliyon 5 (9) (2019), e02415.
[32] A. Taha, M. Ben Aissa, E. Da'na, Green synthesis of an activated carbon-supported Ag and ZnO nanocomposite for photocatalytic degradation and its antibacterial activities, Molecules 25 (7) (2020) 1586.
[33] J.-H. Park, J.-H. Eom, S.-L. Lee, S.-W. Hwang, S.-H. Kim, S.-W. Kang, J.-J. Yun, J.-S. Cho, Y.-H. Lee, D.-C. Seo, Exploration of the potential capacity of fly ash and bottom ash derived from wood pellet-based thermal power plant for heavy metal removal, Sci. Total Environ. 740 (2020), 140205.
[34] M.G. Xavier, S.F. Banda, Specific surface area and porosity measurements of aluminosilicate adsorbents, Orient. J. Chem. 32 (2016) 2401–2406.
[35] M. Shafiee, R. Foroutan, K. Fouladi, M. Ahmadlouydarab, B. Ramavandi, S. Sahebi, Application of oak powder/Fe3O4 magnetic composite in toxic metals removal from aqueous solutions, Adv. Powder Technol. 30 (3) (2019) 544–554.
[36] B.O. Otunola, O.O. Ololade, A review on the application of clay minerals as heavy metal adsorbents for remediation purposes, Environ. Technol. Innovat. 18 (2020), 100692.
[37] O.E.A. Salam, N.A. Reiad, M.M. ElShafei, A study of the removal characteristics of heavy metals from wastewater by low-cost adsorbents, J. Adv. Res. 2 (4) (2011) 297–303.
[38] K. Zombe, J. Nyirenda, A. Lumai, H. Phiri, Impact of solvent type on total phenol and flavonoid content and sun protection factor of crude cashew nutshell liquid, Sustain. Chem. 3 (3) (2022) 334–344.
[39] A.H. Jawad, S.A. Mohammed, M.S. Mastuli, M.F. Abdullah, Carbonization of corn (Zea mays) cob agricultural residue by one-step activation with sulfuric acid for methylene blue adsorption, Desalination Water Treat. 118 (2018) 342–351.
[40] M. Kigozi, R. Kali, A. Bello, B. Padya, G.M. Kalu-Uka, J. Wasswa, P.K. Jain, P. A. Onwualu, N.Y. Dzade, Modified activation process for supercapacitor electrode materials from African maize cob, Materials 13 (23) (2020) 5412.
[41] C. Tejada-Tovar, Á. Villabona-Ortíz, A.D. Gonzalez-Delgado, A. Herrera, A. Viera De la Voz, Efficient sulfate adsorption on modified adsorbents prepared from Zea mays stems, Appl. Sci. 11 (4) (2021) 1596.
[42] J. Nyirenda, K. Zombe, G. Kalaba, C. Siabbamba, I. Mukela, Exhaustive valorization of cashew nut shell waste as a potential bioresource material, Sci. Rep. 11 (1) (2021) 1–14.
[43] U. Zulfiqar, T. Subhani, S.W. Husain, Synthesis of silica nanoparticles from sodium silicate under alkaline conditions, J. Sol. Gel Sci. Technol. 77 (3) (2016) 753–758.
[44] A. Hebeish, M. El-Rafie, M. El-Sheikh, A.A. Seleem, M.E. El-Naggar, Antimicrobial wound dressing and anti-inflammatory efficacy of silver nanoparticles, Int. J. Biol. Macromol. 65 (2014) 509–515.
[45] X.-F. Zhang, Z.-G. Liu, W. Shen, S. Gurunathan, Silver nanoparticles: synthesis, characterization, properties, applications, and therapeutic approaches, Int. J. Mol. Sci. 17 (9) (2016) 1534.
[46] K. Anandalakshmi, J. Venugobal, V. Ramasamy, Characterization of silver nanoparticles by green synthesis method using Pedalium murex leaf extract and their antibacterial activity, Appl. Nanosci. 6 (3) (2016) 399–408.
[47] M. Amin, F. Anwar, M.R.S.A. Janjua, M.A. Iqbal, U. Rashid, Green synthesis of silver nanoparticles through reduction with Solanum xanthocarpum L. berry extract: characterization, antimicrobial and urease inhibitory activities against Helicobacter pylori, Int. J. Mol. Sci. 13 (8) (2012) 9923–9941.
[48] T. Gholami, M. Salavati-Niasari, M. Bazarganipour, E. Noori, Synthesis and characterization of spherical silica nanoparticles by modified Stöber process assisted by organic ligand, Superlattice. Microst. 61 (2013) 33–41.
[49] J. Verma, A. Bhattacharya, Analysis on synthesis of silica nanoparticles and its effect on growth of T. Harzianum & Rhizoctonia species, Biomed. J. Sci. Tech. Res. 10 (4) (2018) 7890–7897.
[50] G. Sapra, V. Chaudhary, P. Kumar, P. Sharma, A. Saini, Recovery of silica nanoparticles from waste PV modules, Mater. Today Proc. 45 (2021) 3863–3868.
[51] S. Azarshin, J. Moghadasi, Z.A. Aboosadi, Surface functionalization of silica nanoparticles to improve the performance of water flooding in oil wet reservoirs, Energy Explor. Exploit. 35 (6) (2017) 685–697.
[52] A. Mourhly, M. Khachani, A.E. Hamidi, M. Kacimi, M. Halim, S. Arsalane, The synthesis and characterization of low-cost mesoporous silica SiO2 from local pumice rock, Nanomater. Nanotechnol. 5 (2015) 35.
[53] B. Purnawira, H. Purwaningsih, Y. Ervianto, V. Pratiwi, D. Susanti, R. Rochiem, A. Purniawan, Synthesis and characterization of mesoporous silica nanoparticles (MSNp) MCM 41 from natural waste rice husk, in: IOP Conference Series: Materials Science and Engineering, IOP Publishing, 2019.
[54] S. Mukherji, S. Bharti, G. Shukla, S. Mukherji, Synthesis and characterization of size-and shape-controlled silver nanoparticles, Phys. Sci. Rev. 4 (1) (2018).
[55] A. Hebeish, M. El-Rafie, M. El-Sheikh, M.E. El-Naggar, Nanostructural features of silver nanoparticles powder synthesized through concurrent formation of the nanosized particles of both starch and silver, J. Nanotechnol. (2013), 2013.
[56] P. Sibiya, M. Moloto, Effect of precursor concentration and pH on the shape and size of starch capped silver selenide (Ag2Se) nanoparticles, Chalcogenide Lett. 11 (11) (2014).
[57] S. Saputro, L. Mahardiani, M. Masykuri, A. Jazuli, The effectiveness of the activated carbon from coconut shell and corn cob to adsorb Pb (II) ion and it's analysis using solid-phase spectrophotometry, in: IOP Conference Series: Materials Science and Engineering, IOP Publishing, 2019.
[58] C. Yu, H. Wang, M. Lu, F. Zhu, Y. Yang, H. Huang, C. Zou, J. Xiong, Z. Zhong, Application of rice straw, corn cob, and Lotus leaf as agricultural waste derived catalysts for low temperature SCR process: optimization of preparation process, catalytic activity and characterization, Aerosol Air Qual. Res. 20 (4) (2020) 862–876.
[59] A.H. Jawad, A.S. Abdulhameed, M.S. Mastuli, Acid-factionalized biomass material for methylene blue dye removal: a comprehensive adsorption and mechanism study, J. Taibah Univ. Sci. 14 (1) (2020) 305–313.
[60] A. Mbozi, Molecularly-imprinted Polyaniline Nanoparticles for Detection of Aldrin, University of Zambia, 2016.
[61] S. Mwale, M. Munyati, J. Nyirenda, Preparation, characterization, and optimization of a porous polyaniline-copper anode microbial fuel cell, J. Solid State Electrochem. 25 (2) (2021) 639–650.
[62] C.Y. Jung, J.S. Kim, T.S. Chang, S.T. Kim, H.J. Lim, S.M. Koo, One-step synthesis of structurally controlled silicate particles from sodium silicates using a simple precipitation process, Langmuir 26 (8) (2010) 5456–5461.
[63] C.N.H. Thuc, H.H. Thuc, Synthesis of silica nanoparticles from Vietnamese rice husk by sol–gel method, Nanoscale Res. Lett. 8 (1) (2013) 1–10.
[64] A.L. Nogueira, R.A. Machado, A.Z. de Souza, F.V. Martinello, C.s.V. Franco, G. B. Dutra, Synthesis and characterization of silver nanoparticles produced with a bifunctional stabilizing agent, Ind. Eng. Chem. Res. 53 (9) (2014) 3426–3434.
[65] S. Bykkam, M. Ahmadipour, S. Narisngam, V.R. Kalagadda, S.C. Chidurala, Extensive studies on X-ray diffraction of green synthesized silver nanoparticles, Adv. Nanoparticles 4 (1) (2015) 1–10.
[66] D.C. Manatunga, R.M. de Silva, K.N. de Silva, Double layer approach to create durable superhydrophobicity on cotton fabric using nano silica and auxiliary non fluorinated materials, Appl. Surf. Sci. 360 (2016) 777–788.
[67] J. Santos, À. Barreto, J. Nogueira, A.L. Daniel-da-Silva, T. Trindade, M.J. Amorim, V.L. Maria, Effects of amorphous silica nanopowders on the avoidance behavior of five soil species—a screening study, Nanomaterials 10 (3) (2020) 402.
[68] J. Piccin, G. Dotto, L. Pinto, Adsorption isotherms and thermochemical data of FD&C Red n 40 binding by chitosan, Braz. J. Chem. Eng. 28 (2) (2011) 295–304.
[69] I. Ahmad, W. Siddiqui, T. Ahmad, Synthesis, characterization of silica nanoparticles and adsorption removal of Cu2+ ions in aqueous solution, Int. J. Emerg. Technol. Adv. Eng. 7 (8) (2017) 439–445.
[70] W. Zhu, J. Wang, D. Wu, X. Li, Y. Luo, C. Han, W. Ma, S. He, Investigating the heavy metal adsorption of mesoporous silica materials prepared by microwave synthesis, Nanoscale Res. Lett. 12 (1) (2017) 1–9.
[71] G. Jain, Removal of Copper and Zinc from Wastewater Using Chitosan, 2013.
[72] U. Maheshwari, Removal of Metal Ions from Wastewater Using Adsorption: Experimental and Theoretical Studies, BITS, 2015.
[73] O. Üner, Ü. Geçgel, Y. Bayrak, Adsorption of methylene blue by an efficient activated carbon prepared from Citrullus lanatus rind: kinetic, isotherm, thermodynamic, and mechanism analysis, Water Air Soil Pollut. 227 (7) (2016) 247.
[74] S.I. Abubakar, M.B. Ibrahim, Adsorption of bromophenol blue and bromothymol blue dyes onto raw maize cob, Bayero J. Pure Appl. Sci. 11 (1) (2018) 273–281.
[75] Ü. Geçgel, G. Özcan, G.Ç. Gürpınar, Removal of methylene blue from aqueous solution by activated carbon prepared from pea shells (Pisum sativum), J. Chem. (2013), 2013.
[76] A.V. Russakova, L.S. Altynbaeva, M. Barsbay, D.A. Zheltov, M.V. Zdorovets, A. A. Mashentseva, Kinetic and isotherm study of as (III) removal from aqueous solution by pet track-etched membranes loaded with copper microtubes, Membranes 11 (2) (2021) 116.
[77] E. Worch, 3 Adsorption equilibrium I: general aspects and single-solute adsorption, in: Adsorption Technology in Water Treatment, De Gruyter, 2021, pp. 49–88.
[78] M. Abbas, Modeling of adsorption isotherms of heavy metals onto Apricot stone activated carbon: two-parameter models and equations allowing determination of thermodynamic parameters, Mater. Today Proc. 43 (2021) 3359–3364.
[79] B. Meroufel, O. Benali, M. Benyahia, Y. Benmoussa, M. Zenasni, Adsorptive removal of anionic dye from aqueous solutions by Algerian kaolin: characteristics, isotherm, kinetic and thermodynamic studies, J. Mater. Environ. Sci. 4 (3) (2013) 482–491.
[80] S. Khamkure, S.E. Garrido-Hoyos, P. Gamero-Melo, A. Reyes-Rosas, Synthesis and characterization of magnetic xerogel monolith as an adsorbent for as (V) removal from groundwater, Processes 9 (2) (2021) 386.
[81] T.Z.E. Lee, J. Zhang, Y. Feng, X. Lin, J. Zhou, Adsorption of Cd (II) ions by coconut copra: isotherm and regeneration studies, in: IOP Conference Series: Earth and Environmental Science, IOP Publishing, 2021.
[82] A. Hashem, A. Fletcher, A. Safri, A. Ghith, D. Hussein, Carbamoylethylated wood pulp as a new sorbent for removal of Hg (II) from contaminated water: isotherm and kinetic studies, J. Polym. Environ. 29 (3) (2021) 881–891.
[83] M. Temkin, V. Pyzhev, Kinetics of the synthesis of ammonia on promoted iron catalysts, Acta Physicochim. 12 (1) (1940) 217–222.
[84] S.K. Lagergren, About the theory of so-called adsorption of soluble substances, Sven. Vetenskapsakad. Handingarl 24 (1898) 1–39.
[85] Y.-S. Ho, G. McKay, Kinetic models for the sorption of dye from aqueous solution by wood, Process Saf. Environ. Protect. 76 (2) (1998) 183–191.
[86] L. Giraldo, A. Erto, J.C. Moreno-Piraján, Magnetite nanoparticles for removal of heavy metals from aqueous solutions: synthesis and characterization, Adsorption 19 (2) (2013) 465–474.

[87] S.K. Lakkaboyana, K. Soontarapa, N.K. Asmel, V. Kumar, R.K. Marella, A. Yuzir, W.Z.W.Y. Zuhairi, Synthesis and characterization of Cu (OH) 2-NWs-PVA-AC Nano-composite and its use as an efficient adsorbent for removal of methylene blue, Sci. Rep. 11 (1) (2021) 1–17.
[88] H.K. Al-Hakeim, I.M. Al-Dahan, Z. Al-Hillawi, R. Bustan, Interaction of prolactin hormone with the surfaces of two new azo compounds, Int. J. Pharm. Pharmaceut. Sci. 6 (2014) 383–387.
[89] C.W. Lim, T.W. Kim, Dynamic [2] catenation of Pd (II) self-assembled macrocycles in water, Chem. Lett. 41 (1) (2012) 70–72.
[90] A. Alasadi, F. Khaili, A. Awwad, Adsorption of Cu (II), Ni (II) and Zn (II) ions by nano kaolinite: thermodynamics and kinetics studies, Chem. Int. 5 (4) (2019), 258-226.
[91] A.M. Salih, The purification of industrial wastewater to remove heavy metals and investigation into the use of zeolite as a remediation tool, 2018.
[92] S.J. Peighambardoust, R. Foroutan, S.H. Peighambardoust, H. Khatooni, B. Ramavandi, Decoration of Citrus limon wood carbon with Fe3O4 to enhanced Cd2+ removal: a reclaimable and magnetic nanocomposite, Chemosphere 282 (2021), 131088.
[93] S.S. Hosseini, A. Hamadi, R. Foroutan, S.J. Peighambardoust, B. Ramavandi, Decontamination of Cd2+ and Pb2+ from aqueous solution using a magnetic nanocomposite of eggshell/starch/Fe3O4, J. Water Proc. Eng. 48 (2022), 102911.
[94] S. Moussa, M. Ali, R.R. Sheha, The performance of activated carbon/NiFe2O4 magnetic composite to retain heavy metal ions from aqueous solution, Chin. J. Chem. Eng. 29 (2021) 135–145.
[95] K.L. Wasewar, Adsorption of metals onto tea factory waste: a review, Int. J. Recent Res. Appl. Stud. 3 (2010) 303–322.
[96] E.G. El-Ammouri, Heavy metals removal from effluents by adsorption on activated silica sols by Elias El-Ammouri, 2000.
[97] W.H.O, Guidelines for drinking-water quality, WHO Chron. 38 (4) (2011) 104–108.
[98] R. Foroutan, S.J. Peighambardoust, A. Ahmadi, A. Akbari, S. Farjadfard, B. Ramavandi, Adsorption mercury, cobalt, and nickel with a reclaimable and magnetic composite of hydroxyapatite/Fe3O4/polydopamine, J. Environ. Chem. Eng. 9 (4) (2021), 105709.
[99] R. Foroutan, S.J. Peighambardoust, S. Hemmati, H. Khatooni, B. Ramavandi, Preparation of clinoptilolite/starch/CoFe2O4 magnetic nanocomposite powder and its elimination properties for cationic dyes from water and wastewater, Int. J. Biol. Macromol. 189 (2021) 432–442.
[100] R. Foroutan, S.J. Peighambardoust, P. Latifi, A. Ahmadi, M. Alizadeh, B. Ramavandi, Carbon nanotubes/β-cyclodextrin/MnFe2O4 as a magnetic nanocomposite powder for tetracycline antibiotic decontamination from different aqueous environments, J. Environ. Chem. Eng. 9 (6) (2021), 106344.
[101] R. Foroutan, S.J. Peighambardoust, R. Mohammadi, S.H. Peighambardoust, B. Ramavandi, Development of new magnetic adsorbent of walnut shell ash/starch/Fe3O4 for effective copper ions removal: treatment of groundwater samples, Chemosphere 296 (2022), 133978.
[102] R. Foroutan, S.J. Peighambardoust, R. Mohammadi, S.H. Peighambardoust, B. Ramavandi, Cadmium ion removal from aqueous media using banana peel biochar/Fe3O4/ZIF-67, Environ. Res. 211 (2022), 113020.
[103] P.S. Kumar, S. Ramalingam, R. Abhinaya, K. Thiruvengadaravi, P. Baskaralingam, S. Sivanesan, Lead (II) adsorption onto sulphuric acid treated cashew nut shell, Separ. Sci. Technol. 46 (15) (2011) 2436–2449.
[104] P.S. Kumar, S. Ramalingam, R.V. Abhinaya, K.V. Thiruvengadaravi, P. Baskaralingam, S. Sivanesan, Lead(II) adsorption onto sulphuric acid treated cashew nut shell, Separ. Sci. Technol. 46 (15) (2011) 2436–2449.